Systematic Trends for the Medium Field Q-Slope

J. Vines, Y. Xie, H. Padamsee
Cornell University, Ithaca, NY 14853.

Abstract

The medium field Q-slope for Nb cavities has been studied in the past as a thermal feedback effect combined with the nonlinear BCS surface resistance due to current-induced RF pair-breaking. We are systematically exploring the behavior of the medium field Q-slope with various cavity parameters such as wall thickness, residual resistance, bath temperature, Kapitza conductance, RF frequency, RRR, and phonon mean free path. We study cases involving only the standard (linear) BCS resistance as well as those including the nonlinear BCS resistance. The systematic comparison suggests specific experiments to determine the role of the nonlinear contribution.

INTRODUCTION

One of the limiting factors in the performance of superconducting radio-frequency (SRF) cavities is the ability of the cavity walls to transport heat created at the interior surface of the cavity to the surrounding low-temperature bath. If this heat is not dispersed sufficiently rapidly, it can significantly increase the temperature of the cavity, which, in turn, will lead to increased heat production; this process is known as thermal feedback. Since an important goal in cavity performance is to maximize the accelerating field while minimizing heating losses, it is important to understand the quantitative relationship between heat production and the RF fields. This relationship is usually summarized in the quality factor Q of a cavity, which is the number of RF cycles it takes to dissipate all the energy stored in the cavity, and its dependence on the magnitude of the RF field. The dependence of Q on the RF field strength is often represented by a dimensionless parameter γ known as the medium field Q-slope.

In this paper we explore the mechanisms of thermal feedback, with standard and nonlinear BCS resistance cases, and how these mechanisms influence the quality factor of a cavity. In the first section, we review a common theoretical model of the heat flow problem and describe a numerical method for solving the heat flow equations. We also discuss an approximate analytic solution for the case of standard BCS resistance from Halbritter [1] and its derivation. The following section reviews the material properties involved in the thermal feedback model and presents the particular forms of material functions used in our calculations. We then present and discuss the results of numerical calculations of quality factors for various cavity parameters. After briefly comparing these numerical results with experimental data, we summarize our findings for the standard BCS resistance case. Finally, we discuss the impact of the nonlinear BCS resistance.

Understanding and controlling the medium field Q-slope is important to future continuous wave (CW) applications such as the Energy Recovery Linacs (ERL) where cryogenics costs dominate due to CW operation at medium fields (< 20 MV/m). Previous studies on the medium field Q-slope have been conducted by Graber [2], Saito [3], Bauer [4], Ciovati [5], [6], and Visentin [7]. The thermal feedback effect is discussed in [8] where it is called the "global thermal instability" (GTI), first discovered for high frequency (3 GHz) cavities by Graber [2]. A thermal model applied to a 3 GHz case predicts a medium field Q-slope as well as a thermal instability at high fields for 3 GHz cavities. Thermometry results at 3 GHz confirmed the global nature of the thermal instability [2].

The new aspect of our studies is to explore systematic trends in the medium field Q-slope with variations in RF frequency, bath temperature, thermal conductivity, Kapitza conductance, and wall thickness. Our numerical approach also takes into account the full temperature dependences of the thermal conductivity, Kapitza conductance, and surface resistance.

THEORETICAL MODEL FOR HEAT TRANSFER

The Quality Factor and the Medium Field Q-slope

The quality factor Q of a SRF cavity is defined as

$$Q = \frac{\omega_0 U}{P} \tag{1}$$

where ω_0 is the angular frequency of the RF field, U is the total energy stored in the RF field inside the cavity, and P is the total power dissipated in the cavity walls [8]. The stored energy is given by an integral of the magnetic field $\mathbf{H}$ over the volume of the cavity:

$$U = \frac{\mu_0}{2} \int_V |\mathbf{H}|^2 \, dv \tag{2}$$

and the dissipated power can be expressed as an integral of the magnetic field over the interior surface of the cavity:

$$P = \frac{1}{2} \int_S R_s |\mathbf{H}|^2 \, ds \tag{3}$$

This equation defines the surface resistance R_s, discussed in Section . If we take R_s to be constant across the surface, then the quality factor can be written as

$$Q = \frac{G}{R_s} \tag{4}$$

where G is the geometry constant, defined by

$$G = \frac{\mu_0 \omega_0 \int_V |\mathbf{H}|^2 \, dv}{\int_S |\mathbf{H}|^2 \, ds} \tag{5}$$

In this paper, we will be more concerned with the behavior of the surface resistance than that of the geometry constant.

The dependence of the quality factor on the strength of the RF field is most often characterized by the medium field Q-slope, represented by the dimensionless parameter γ, introduced by Halbritter [1]. It is defined via an expansion of the surface resistance R_s in even powers of the peak surface magnetic field B:

$$R_s(B) = R_{s0}\left[1 + \gamma\left(\frac{B}{B_c}\right)^2 + O(B)^4\right] \tag{6}$$

Here, $B_c = 0.2\,\mathrm{T}$ is the thermodynamic critical field of niobium, and R_{s0} is the surface resistance at small magnetic fields (usually, B = 15 mT is chosen to define R_{s0}, since, below this field level, the effects of the low-field Q-increase become important). For many real cavities [9], it has been shown that a power series of R_s also contains odd powers of B; however, Halbritter has shown (as we will review in Section) that an increase in the surface resistance due only to thermal feedback should take the form given in Eq. (6). From Eqs. (4) and (6), we can see that the decrease in the quality factor is given in terms of the medium field Q-slope by

$$Q(B) = \frac{G}{R_{s0}}\left[1 - \gamma\left(\frac{B}{B_c}\right)^2 + O(B)^4\right] \tag{7}$$

Values of the Q-slope γ can be measured experimentally or, as will be done in this paper, estimated from a set of basic cavity parameters by means of numerical calculation or analytic approximation.

Heat Flow Equations

Though most SRF cavities have complex curved geometries, their wall thicknesses are generally small in comparison with the surface curvature; thus, locally, the cavity wall can be modeled as a flat slab. Without much loss of generality, we can take the wall to be an infinite flat slab of niobium of thickness d. This choice makes the heat transport calculation a one-dimensional problem. As shown in Figure 1, we take the coordinate z to be the vertical distance from the top (interior) surface of the cavity. Above this surface is the vacuum which carries the RF field. The bottom (exterior) surface of the cavity is located at $z = d$, and below this is the liquid helium bath.

In this configuration, the temperature distribution within the cavity wall can be specified by a function $T(z)$. For $0 < z < d$, we expect the steady-state temperature distribution $T(z)$ to satisfy the differential equation

$$\frac{d}{dz}\left[\kappa(T)\frac{dT}{dz}\right] = 0 \tag{8}$$

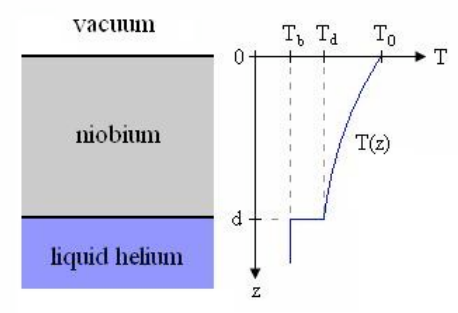

Figure 1: Schematic of the model of the cavity wall as an infinite slab of niobium. Above $z = 0$ is the vacuum which contains the RF field. Below $z = d$ is the liquid helium bath.

where κ is the temperature-dependent thermal conductivity, discussed in Section . The quantity

$$-\kappa(T)\frac{dT}{dz} \equiv q \tag{9}$$

is the heat flux (power per unit area) in the z-direction; this relationship essentially defines thermal conductivity. Thus, Eq. (8) simply expresses the condition that the heat flux q be constant throughout the thickness of the wall, in accordance with the fact that no heat is created or absorbed within the wall in the steady state.

Since Eq. (8) is a second-order differential equation, two boundary conditions are required to fix a unique solution. The first of these can be found by equating the heat flux $q(0)$ at the RF surface to the rate at which heat is being produced at the surface. The mechanism of heat production is essentially Joule heating, caused by surface currents induced by the RF magnetic field. The power dissipated per unit area can be expressed as

$$q = \frac{1}{2}R_s(T_0)H^2 \tag{10}$$

where H is the peak surface magnetic field, and R_s is the surface resistance, which, as indicated, is a function of the temperature $T_0 \equiv T(z = 0)$ at the RF surface. The sources of the surface resistance and its functional form are discussed in Section . Altogether, the boundary condition at $z = 0$ reads

$$-\kappa(T_0)\left.\frac{dT}{dz}\right|_{z=0} = \frac{1}{2}R_s(T_0)H^2 \tag{11}$$

The second boundary condition involves the Kapitza conductance of the niobium-liquid helium interface. When heat flows across an interface between superfluid helium and a metallic solid, there is a discontinuity in temperature at the interface [13]. It has been found that the temperature difference is related to the heat flux q across the surface by

$$q = (T_d - T_b)H_k(T_d, T_b) \tag{12}$$

where T_d is the temperature of the metal at the interface, T_b is the temperature of the superfluid helium bath, and the function H_k, known as the Kapitza conductance, is determined by the nature of the metallic surface. From this, the second boundary condition can be written as

$$-\kappa(T_d)\frac{dT}{dz}\bigg|_{z=d} = (T_d - T_b)H_k(T_d, T_b) \qquad (13)$$

where $T_d \equiv T(z = d)$ is the temperature of the niobium at the interface.

Together, Eqs. (8), (11), and (13) will render a unique solution for $T(z)$, given the material functions $\kappa(T)$, $R_s(T)$, and $H_k(T_d, T_b)$, the bath temperature T_b, and the magnetic field magnitude H. The most useful information from the solution will be the temperature T_0 at the RF surface, which can be used to find the surface resistance and thus the quality factor of a cavity.

Numerical Solution of Heat Flow Equations

One can obtain a numerical solution to the heat flow equations by dividing the niobium slab into a series of small layers and turning the differential equations above into a set of finite-difference equations. We can take the slab of thickness d to be divided into N layers of thickness $\Delta z = d/N$ and label them with the integers i = 0, 1, 2, ... $N-2$, $N-1$. We can take the temperature T_i in layer i to be constant throughout the layer. Then, differential equation (8) can become

$$\frac{d}{dz}\left[\kappa(T)\frac{dT}{dz}\right]_i = \frac{1}{\Delta z}\left[\kappa_i\frac{T_{i+1}-T_i}{\Delta z} - \kappa_{i-1}\frac{T_i - T_{i-1}}{\Delta z}\right] \qquad (14)$$

where κ_i is the thermal conductivity between layers i and $i+1$ and is found by evaluating $\kappa(T)$ at the average temperature of those two layers:

$$\kappa_i = \kappa\left(\frac{T_i + T_{i+1}}{2}\right) \qquad (15)$$

Similarly, the boundary conditions (11) and (13) can be rewritten as

$$-\kappa(T_0)\frac{dT}{dz}\bigg|_{z=0} = -\kappa_0\frac{T_1 - T_0}{\Delta z} = \frac{1}{2}R_s(T_0)H^2 \qquad (16)$$

$$-\kappa(T_d)\frac{dT}{dz}\bigg|_{z=d} = -\kappa_{N-2}\frac{T_{N-1} - T_{N-2}}{\Delta z} = (T_{N-1} - T_b)H_k(T_{N-1}, T_b) \qquad (17)$$

These equations can be rearranged to yield

$$T_0 = \frac{R_s(T_0)H^2\Delta z/2 + \kappa_0 T_1}{\kappa_0} \qquad (18)$$

$$T_i = \frac{\kappa_{i-1}T_{i-1} + \kappa_i T_{i+1}}{\kappa_{i-1} + \kappa_i} \qquad (19)$$

$$T_{N-1} = \frac{\kappa_{N-2}T_{N-2} + H_k(T_{N-1}, T_b)\Delta z T_b}{\kappa_{N-2} + H_k\Delta z} \qquad (20)$$

Here, Eq. (19) applies for $1 \geq i \geq N-2$. Now, even though the temperatures on the left hand sides of the above equations also appear on the right hand sides of these equations, these N equations can be used to define a recursion relation on the set of T_i. Given an initial set of T_i, one can evaluate the right hand sides of the above equations using this set and thus obtain a new set of T_i through these equations. If this process is repeated recursively (being sure to update the values κ_i each time), the set of T_i will converge to a numerical solution of the original differential equation [10]. This iterative solution method has been encoded into to a program in the C++ language, and results obtained from this program are presented below. (The approach adopted here is identical to that used in an earlier effort using the FORTRAN program HEAT [10].)

Analytic Approximation for γ

With a little bit of analytic work on the heat flow equations, we can both justify the quadratic form for $R_s(B)$ in Eq. (6) and obtain an approximate formula for the Q-slope γ (in the standard BCS case) first presented by Halbritter [1]. To proceed, we can recall that the heat flux q in Eq. (9) must be equal to the same constant for all z; also, this constant q should also be equal to both the heat flux resulting from the surface resistance in Eq. (10) and that from the Kapitza conductance in Eq. (12). We can summarize this with the two equations

$$\frac{H^2}{2}R_s(T_0) = (T_d - T_b)H_k(T_d, T_b) \qquad (21)$$

$$(T_d - T_b)H_k(T_d, T_b) = -\kappa(T)\frac{dT}{dz} \qquad (22)$$

The second of these can be integrated with respect to z to give

$$\int_0^d (T_d - T_b)H_k(T_d, T_b)\,dz = -\int_0^d \kappa(T)\frac{dT}{dz}\,dz$$

$$\Rightarrow \quad (T_d - T_b)H_k(T_d, T_b)d = -\int_{T_0}^{T_d}\kappa(T)\,dT \qquad (23)$$

Now, we must make some assumptions and approximations to make progress. First, we assume that the variations in temperature, i.e. $T_0 - T_b$ and $T_d - T_b$, are small compared with T_b. If this is the case, we can approximate the thermal conductivity and the Kapitza conductance with their values at $T_0 = T_b$ and $T_d = T_b$; this is convenient because the bath temperature T_b is known a priori. Making this approximation also requires that the Kapitza conductance function be non-zero when its two arguments are equal. (As we will see below, this is only the case below the lambda point of superfluid helium, whereas, at higher temperatures, $H_k(T, T) = 0$ and this approximation scheme will breakdown.)

So, assuming we can do so, we replace $\kappa(T)$ and $H_k(T_d, T_b)$ in Eq. (23) with the constants $\kappa \equiv \kappa(T_b)$ and

$H_k \equiv H_k(T_b, T_b)$ to give

$$H_k d(T_d - T_b) = -\kappa \int_{T_0}^{T_d} dT = \kappa(T_0 - T_d) \quad (24)$$

which allows us to solve for T_d:

$$T_d = \frac{H_k d T_b + \kappa T_0}{H_k d + \kappa} \quad (25)$$

This expression for T_d can now be substituted into Eq. (21), where we also replace $H_k(T_d, T_b)$ with H_k, giving

$$\frac{H^2}{2} R_s(T_0) = \frac{\kappa H_k}{\kappa + H_k d}(T_0 - T_b) \quad (26)$$

or, defining

$$\alpha \equiv \frac{\kappa H_k}{\kappa + H_k d} \quad (27)$$

we have

$$\frac{H^2}{2} R_s(T_0) = \alpha(T_0 - T_b) \quad (28)$$

At this point, we must use an approximation to the surface resistance $R_s(T_0)$. Saying $R_s(T_0) = R_s(T_b)$ as we did for the thermal conductivity and Kapitza conductance would not suffice, for in that case, $R_s(T_0)$ would not depend on the magnetic field. Instead, we can make a linear approximation to $R_s(T_0)$ around T_b:

$$R_s(T_0) = R_s(T_b) + \left(\frac{dR_s}{dT}\right)_{T=T_b} (T_0 - T_b) \quad (29)$$

(One might say that going to first order in ΔT for R_s while we only went to zeroth order in ΔT for κ and H_k is inconsistent; however, for the particular cases we'll consider, the variation of R_s with tempature is much more dramatic than that of κ or H_k, so we are at least somewhat justified.) To evaluate the derivative in this equation, we must assume an explicit form for the surface resistance. The major features of the dependence of R_s on T can be summarized in the approximate equation

$$R_s(T) = R_0 + R_{BCS}(T) = R_0 + C \exp\left(-\frac{\Delta}{k_B T}\right) \quad (30)$$

Here, Δ is the superconductor energy gap, which is roughly constant for $T < T_c/2$, and R_0 and C are constants. From this, we can evaluate the derivative

$$\left(\frac{dR_s}{dT}\right)_{T=T_b} = \frac{\Delta}{k_B T_b^2} R_{BCS}(T_b) \quad (31)$$

and plug it into Eq. (29) to find

$$R_s(T_0) = R_s(T_b) + \frac{\Delta}{k_B T_b^2} R_{BCS}(T_b)(T_0 - T_b) \quad (32)$$

Now, this expression for $R_s(T_0)$ can be inserted into Eq. (28), resulting in

$$\frac{H^2}{2}\left[R_s(T_b) + \frac{\Delta}{k_B T_b^2} R_{BCS}(T_b)(T_0 - T_b)\right] = \alpha(T_0 - T_b) \quad (33)$$

which can be solved for T_0:

$$T_0 = \frac{\frac{H^2}{2}\left[R_s(T_b) - \frac{\Delta}{k_B T_b} R_{BCS}(T_b)\right] + \alpha T_b}{\alpha - \frac{H^2}{2}\frac{\Delta}{k_B T_b^2} R_{BCS}(T_b)} \quad (34)$$

With this expression for the surface temperature T_0 solely in terms of the bath temperature T_b, the magnetic field H, and material functions, we have (approximately) solved the problem at hand. To find the surface resistance, we can simply plug Eq. (34) for T_0 into Eq. (28); after a bit of simplification, one finds

$$R_s(T_0) = R_s(T_b)\left[1 - \frac{H^2}{2}\frac{\Delta}{k_B T_b^2} R_{BCS}(T_b)\frac{1}{\alpha}\right]^{-1} \quad (35)$$

If we assume that the quantity subtracted from 1 here is small (which it should be, since it's proportional to H^2 and we are looking for the medium field behavior), then we can use $(1-x)^{-1} \approx 1+x$. Then, after replacing H with B/μ_0, adding in some cosmetic critical fields B_c, and plugging in Eq. (27) for α, we find $R_s(T_0) =$

$$R_s(T_b)\left[1 + \frac{B_c^2}{2\mu_0^2}\frac{\Delta}{k_B T_b^2} R_{BCS}(T_b)\left(\frac{d}{\kappa} + \frac{1}{H_k}\right)\left(\frac{B}{B_c}\right)^2\right] \quad (36)$$

This expression has precisely the same form as that in Eq. (6); we have thus given somewhat of a justification for the quadratic dependence of R_s on B postulated there. Identifying $R_s(T_b)$ in Eq. (36) with R_{s0} in Eq. (6), the coefficient of $(B/B_c)^2$ in Eq. (36) should be identified with γ in Eq. (6). Thus, we have arrived at an approximate analytic expression for the medium field Q-slope γ:

$$\gamma = \frac{B_c^2}{2\mu_0^2}\frac{\Delta}{k_B T_b^2} R_{BCS}(T_b)\left(\frac{d}{\kappa} + \frac{1}{H_k}\right) \quad (37)$$

This is the formula for the Q-slope presented by Halbritter [1].

MATERIAL PROPERTIES

Thermal Conductivity

For the niobium thermal conductivity, we use an analytic expression presented by Koechlin and Bonin [11]. Their formula is based on a theoretical model of heat conduction by electons and phonons and includes constants obtained from fitting to experimental data. The expression involves three free parameters: the temperature T, the residual resistivity ratio RRR, and the mean free path of lattice phonons l. RRR is a commonly used measure of the purity of a niobium sample and is defined as the ratio of the electrical resistivity at room temperature to the residual (low temperature limit) resistivity. The phonon mean free path l may also be influenced by strains and dislocations but, for relatively pure samples, is roughly equal to the average grain size.

In the normal state ($T \geq T_c = 9.25$K), they write the thermal conductivity as

$$\kappa_n(T, RRR, l) = \left[\frac{1}{A\,RRR\,T} + aT^2\right]^{-1} + \left[\frac{1}{DT^2} + \frac{1}{BlT^3}\right]^{-1} \quad (38)$$

and, in the superconducting state ($T \leq T_c$), as

$$\kappa_s(T, RRR, l) = R(y)\left[\frac{1}{A\,RRR\,T} + aT^2\right]^{-1} + \left[\frac{1}{DT^2 e^y} + \frac{1}{BlT^3}\right]^{-1} \quad (39)$$

Here, y is the superconductor energy gap divided by $k_B T$, which can be approximated by

$$y = \frac{\Delta(T)}{k_B T} \approx \frac{\Delta(0)}{k_B T}\left[\cos\left(\frac{\pi T^2}{2T_c^2}\right)\right]^{1/2} \quad (40)$$

and the function $R(y)$ is given by

$$R(y) = \frac{12}{\pi^2}\left[f(y) + y\ln(1+e^{-y}) + \frac{y^2/2}{1+e^y}\right] \quad (41)$$

with

$$f(y) = \int_0^\infty \frac{z\,dz}{1+e^{z+y}} \quad (42)$$

The constants, as found by Koechlin and Bonin, are

$$A = 0.141\ \mathrm{W\,K^{-2}\,m^{-1}} \quad (43)$$
$$a = 7.52\times10^{-7}\ \mathrm{W^{-1}\,K^{-1}\,m} \quad (44)$$
$$B = 4.34\times10^{3}\ \mathrm{W\,K^{-4}\,m^{-2}} \quad (45)$$
$$1/D = 2.34\times10^{2}\ \mathrm{W^{-1}\,K^{3}\,m} \quad (46)$$

In the normal state, the electron contribution [the first of the two brackets in Eq. (38)] dominates the thermal conductivity, and it increases monotonically with temperature. However, in the superconducting state, for sufficiently large phonon mean free paths, the phonon contribution (the second bracket) can lead to a local maximum in the thermal conductivity as a function of temperature, known as a phonon peak. The height of the phonon peak increases with increasing values of l. For all values of l and T, an increase in RRR produces an increase in the thermal conductivity. Figures 2 and 3 demonstrate these behaviors with plots of $\kappa(T)$ for various values of l and RRR.

Experience shows that most fine grain Nb has no phonon peak, due to the phonon mean free path being comparable to the grain size (< 0.1 mm). Post purified cavities are expected to have a phonon peak due to grain growth to 1-2 mm. Large grain Nb has a phonon peak which can easily be depressed by a small amount of strain ($< 10\%$) [12]. However we can expect that some or all of the phonon peak may re-appear after 800 C annealing as most cavities receive for H degassing. Hence there is a large range in the expected size of the phonon peak for Nb cavities depending strongly on how the cavity has been prepared.

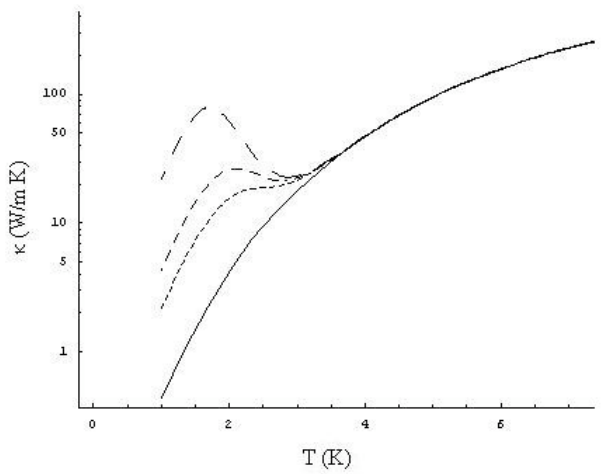

Figure 2: Thermal conductivity versus temperature for RRR = 300 and l = 0.1 mm (solid), 0.5 mm (short dashed), 1.0 mm (medium dashed), and 5.0 mm (long dashed).

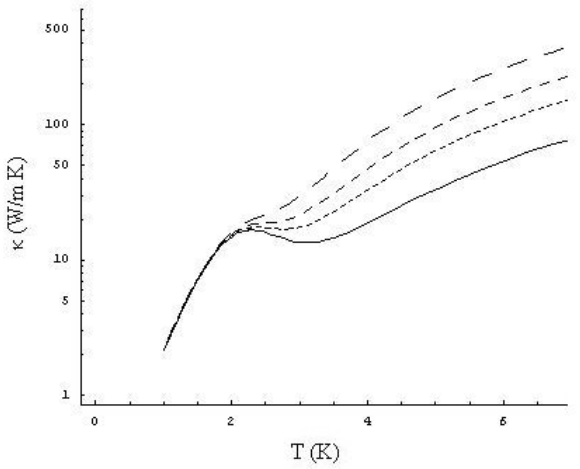

Figure 3: Thermal conductivity versus temperature for l = 0.5 mm and RRR = 100 (solid), 200 (short dashed), 300 (medium dashed), and 500 (long dashed).

Surface Resistance

The surface resistance of a niobium cavity can be written as a sum of two contributions:

$$R_s(T) = R_0 + R_{BCS}(T) \quad (47)$$

The temperature-independent residual resistance R_0 can arise from any number of sources, such as foreign material inclusions or condensed gases, and is typically around the range 5-20 nΩ [8]. The BCS resistance R_{BCS} arises from the motion of normal electrons near the RF surface; it can be calculated from the BCS theory of superconductivity but generally has a rather complicated form. For the

section on standard BCS resistance, we will use a Pippard approximation for R_{BCS} [10]:

$$R_{BCS}(T) = (2.78 \times 10^{-5}\,\Omega)\,\frac{\nu^2}{t}\ln\left(\frac{148t}{\nu}\right)\exp\left[-\frac{1.81g(t)}{t}\right] \quad (48)$$

$$t = \frac{T}{T_c}\ , \quad \nu = \frac{f}{2.86\,\mathrm{GHz}}\ , \quad g(t) = \left[\cos\left(\frac{\pi t^2}{2}\right)\right]^{1/2} \quad (49)$$

where f is the frequency of the RF field. Here, we can see that the BCS resistance increases exponentially with temperature in the superconducting state.

Kapitza Conductance

Below, we will use three different forms for the Kapitza conductance H_k, each obtain from fits to experimental data [13]. The first of these has been obtained from data on unannealed (UA) niobium interfacing with superfluid helium:

$$H_k(T_d, T_b) = \left(170\ \frac{\mathrm{W}}{\mathrm{m^2K}}\right)\left(\frac{T_b}{1\,\mathrm{K}}\right)^{3.62} f(t) \quad (50)$$

where

$$f(t) = 1 + \frac{3}{2}t + t^2 + \frac{1}{4}t^3 \quad , \quad t = \frac{T_d - T_b}{T_b} \quad (51)$$

The second comes from measurements on annealed (A) niobium interfacing with superfluid helium:

$$H_k(T_d, T_b) = \left(200\ \frac{\mathrm{W}}{\mathrm{m^2K}}\right)\left(\frac{T_b}{1\,\mathrm{K}}\right)^{4.65} f(t) \quad (52)$$

where $f(t)$ is again given by Eq. (51). Finally, we have an expression for the heat conductance when the bath temperature has exceeded the superfluid lambda point (2.18 K) and the helium has begun to nucleate and boil (NB):

$$H_k(T_d, T_b) = \left(1.2 \times 10^4\ \frac{\mathrm{W}}{\mathrm{m^2K}}\right)\left(\frac{T_d - T_b}{1\,\mathrm{K}}\right)^{0.45} \quad (53)$$

So, we have two conductances that apply below 2.18 K, (UA) and (A), and one that applies above 2.18 K, (NB). To compare the three formulae, we can plot the heat flux $q = (T_d - T_b)H_k(T_d, T_b)$ across the interface as a function of the temperature difference $\Delta T = T_d - T_b$, for each of the three functions above, all with a bath temperature of 2.18 K. This is shown in Figure 4. It is clear that annealed niobium results in the best heat conduction to the bath, followed by unannealed niobium (for low enough ΔT). Another important feature to note from this figure is that the nucleate boiling curve has zero slope at $\Delta T = 0$, or in other words, the heat conductance H_k is zero there. This means that the analysis in Section that led to a quadratic $R_s(B)$ and Halbritter's formula for γ would break down in the case of nucleate boiling conductance.

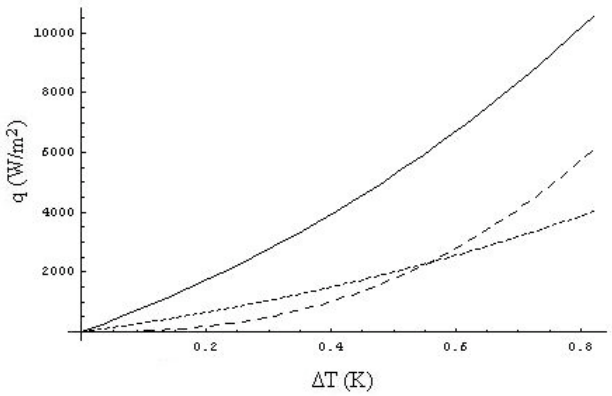

Figure 4: Thermal conductance across Nb-LHe interface as a function of temperature difference for annealed niobium (solid), unannealed niobium (short dashed), and nucleate boiling (long dashed).

NUMERICAL RESULTS

Figures 5, 7, 9, 11, 13, 15, and 17 summarize the results of numerical calculations of Q values in the standard BCS case for various properties of niobium cavities. In each figure, one of the following cavity properties is varied while the others are held fixed at the baseline values given here in parentheses:

- RF frequency f (1.3 GHz)
- Helium bath temperature T_b (1.8 K)
- Residual resistance R_0 (10 nΩ)
- Wall thickness d (3 mm)
- Residual resistivity ratio RRR (300)
- Phonon mean free path l (0.1 mm)

The only exception to this pattern is Figure 17, where T_b = 2.18 K, the lambda point of superfluid helium, instead of 1.8 K; all other parameters have the baseline values.

Figures 6, 8, 10, 12, 14, 16, and 18 display γ values computed for each of these cases. They were calculated from a least-squares fit to Eq. (6) of the numerical values obtained for $R_s(B)$ up to $B = 0.1$ T. In general, the quadratic fit to $R_s(B)$ worked very well, with an average of $R^2 = 0.92$. These figures also display the corresponding γ values computed from Halbritter's approximate formula in Eq. (37). It is clear from the figures that this formula is an excellent appoximation for almost all cases; the rms deviation between Halbritter's formula and the numerical results is 5.6%. However, in the case of nucleate boiling heat transfer at the Nb-LHe interface, Halbritter's formula is not applicable, since $H_k = 0$ implies $\gamma = \infty$.

In Figures 5 and 6, we see that the baseline Q values decrease and γ increases with increasing RF frequency f, as is to be expected from the f^2 increase of the BCS surface resistance. Though the Q-slopes shown in these figures (and others) may seem atypically dramatic when compared

to experimental observation, it is important to note that, in all these cases, the phonon mean free path l has been set to 0.1 mm, in which case there is no phonon peak in the thermal conductivity, corresponding to fine grain Nb that has not been post-purified. It is also important to note that the high field Q-slope phenomena take over above $B = 0.1$ T, and thus the medium field Q-slope calculations are probably relevant above $B = 0.1$ T only for electropolished (EP) cavities which have been baked at 100-120 C where the high field Q-slope disappears [14]. For the higher frequencies shown in Figure 5, we see behavior that resembles a high field Q-drop, even though only thermal effects have been considered in these calculations.

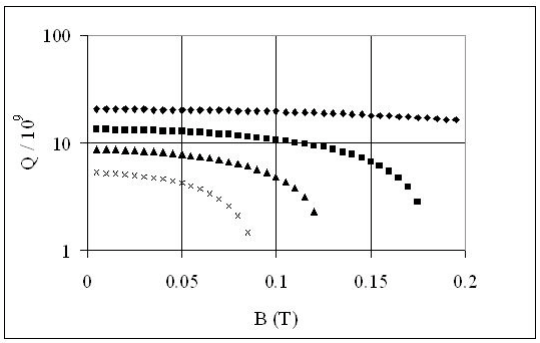

Figure 5: Variation of quality factor with magnetic field for RF frequencies f = 0.6 GHZ (♦), 1.3 GHz (■), 2.0 GHz (▲), and 3.0 GHz (×).

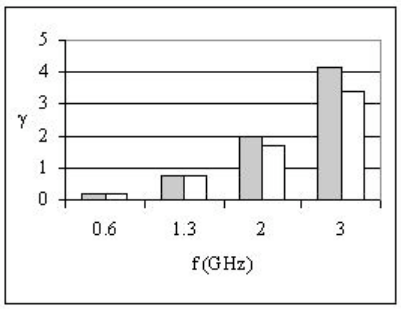

Figure 6: Medium field Q-slope values for varying RF frequency f, calculated numerically (shaded) and from Halbritter's approximate formula (unshaded).

The variation of Q and γ with wall thickness d is shown in Figures 7 and 8. For low magnetic fields, the Q values are largely independent of d; for higher fields, a smaller wall thickness improves Q values and thus decreases γ. An intuitive explanation for this is that bringing the helium bath closer to the RF surface helps the cooling process.

In Figures 9 and 10, we see a decrease in baseline Q values and an increase in γ values with increasing residual resistance R_0, due to added heating from the extra surface resistance. Here, we see a difference in trends between the

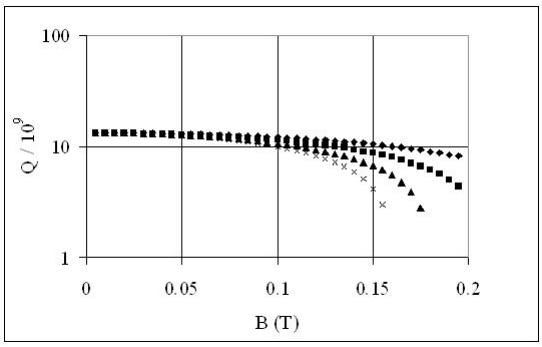

Figure 7: Variation of quality factor with magnetic field for wall thicknesses d = 1 mm (♦), 2 mm (■), 3 mm (▲), and 4 mm (×).

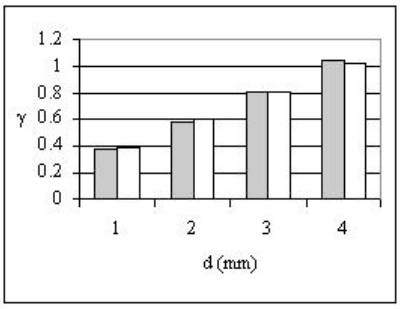

Figure 8: Medium field Q-slope values for varying wall thickness d, calculated numerically (shaded) and from Halbritter's approximate formula (unshaded).

numerical results and Halbritter's formula: Halbritter's formula predicts that γ will be independent of R_0, while the numerical results show it increasing, though very slightly, with R_0.

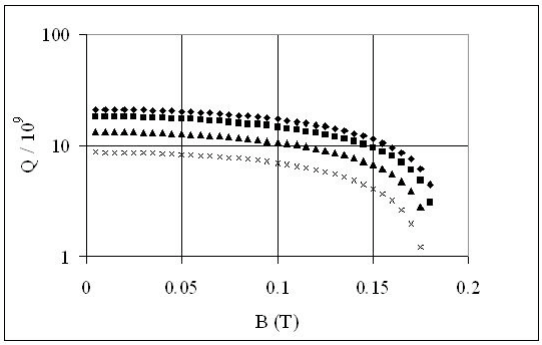

Figure 9: Variation of quality factor with magnetic field for residual resistances R_0 = 3 nΩ (♦), 5 nΩ (■), 10 nΩ (▲), and 20 nΩ (×).

We see in Figures 11 and 12 that the Q-slope is only slightly improved when RRR is increased. This is consis-

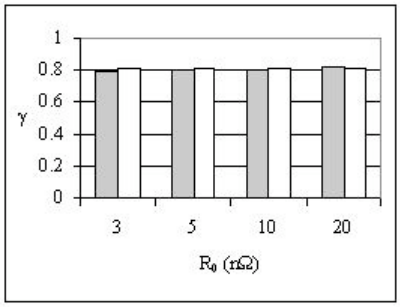

Figure 10: Medium field Q-slope values for varying residual resistance R_0, calculated numerically (shaded) and from Halbritter's approximate formula (unshaded).

tent with the fact that, below 2 K, the thermal conductivity is mostly determined by the value of the phonon mean free path l, as demonstrated in Figures 2 and 3. In Figures 13 and 14, we see a decrease in baseline Q values and an increase in γ values with increasing bath temperature.

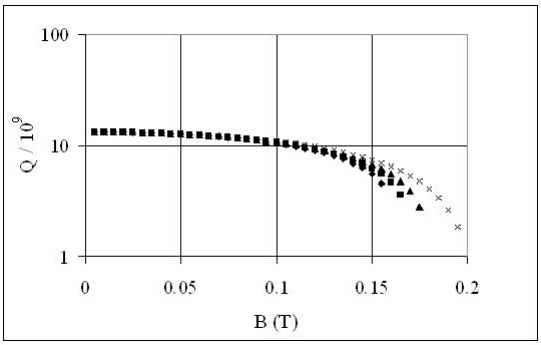

Figure 11: Variation of quality factor with magnetic field for residual resistivity ratios RRR = 100 (♦), 200 (■), 300 (▲), and 500 (×).

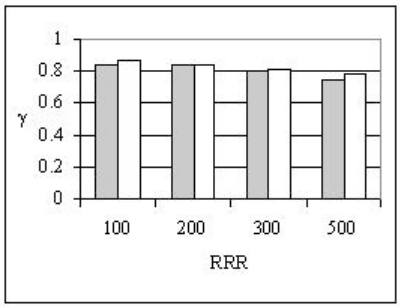

Figure 12: Medium field Q-slope values for varying residual resistivity ratio RRR, calculated numerically (shaded) and from Halbritter's approximate formula (unshaded).

Figures 15 and 16 show the variation of Q and γ values with the phonon mean free path l, which, as discussed

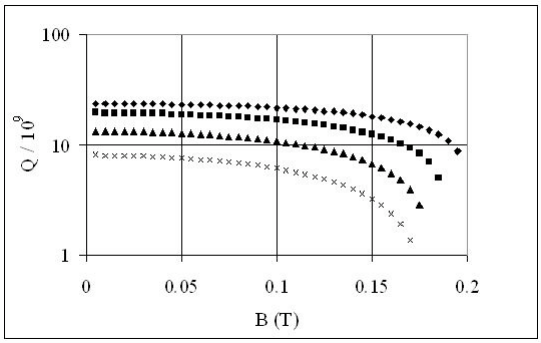

Figure 13: Variation of quality factor with magnetic field for bath temperatures T_b = 1.4 K (♦), 1.6 K (■), 1.8 K (▲), and 2.0 K (×).

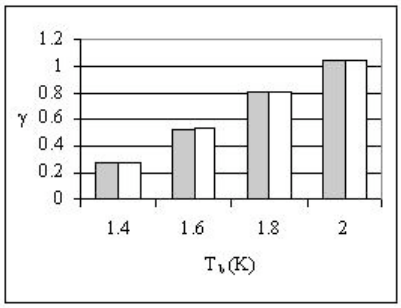

Figure 14: Medium field Q-slope values for varying bath temperature T_b, calculated numerically (shaded) and from Halbritter's approximate formula (unshaded).

above, can generally be associated with the average grain size of the niobium sample. It is clear that increasing the grain size, and thus introducing a larger phonon peak in the thermal conductivity, will decrease γ values and can remove medium field Q-slopes that are present in samples with smaller grain sizes. These results demonstrate that it is important to know the treatment history of a given sample, since *an estimation of its phonon mean free path is crucial to analyzing the results of* Q *and* γ *measurements.*

Finally, in Figures 17 and 18, we have Q and γ values for the three different thermal conductance functions. As expected, we see that the annealed niobium has a lower γ value than the unannealed niobium. The most interesting point here, though, is that the $Q(B)$ curve for the nucleate boiling conductance shows more of a linear behavior than a quadratic one (that is, dQ/dB at $B = 0$ is not zero, as it should be according to Eq. (6)), hence the huge γ value. However, this is not all that unexpected, since, as noted above, the derivation of the quadratic form for $Q(B)$ in Eq. (6) breaks down when $H_k(T, T) = 0$, as is the case for the nucleate boiling conductance.

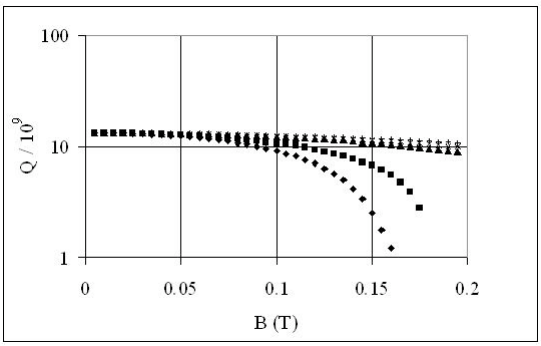

Figure 15: Variation of quality factor with magnetic field for phonon mean free paths l = 0.05 mm (♦), 0.1 mm (■), 0.5 mm (▲), 1.0 mm (×), and 5.0 mm (+).

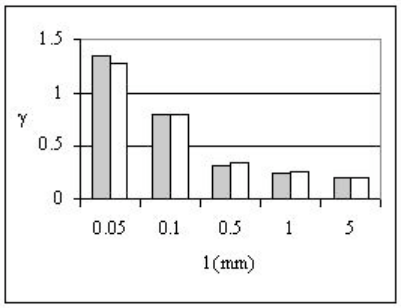

Figure 16: Medium field Q-slope values for varying phonon mean free path l, calculated numerically (shaded) and from Halbritter's approximate formula (unshaded).

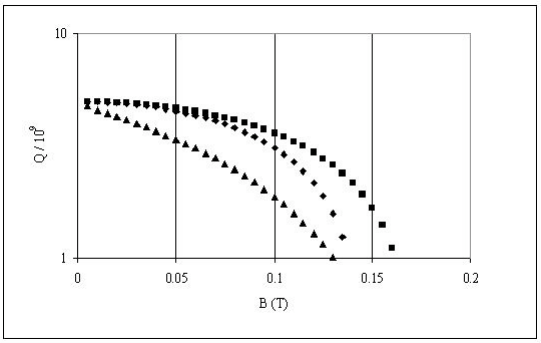

Figure 17: Variation of quality factor with magnetic field for thermal conductances of unannealed niobium (♦), annealed niobium (■), and nucleate boiling helium (▲).

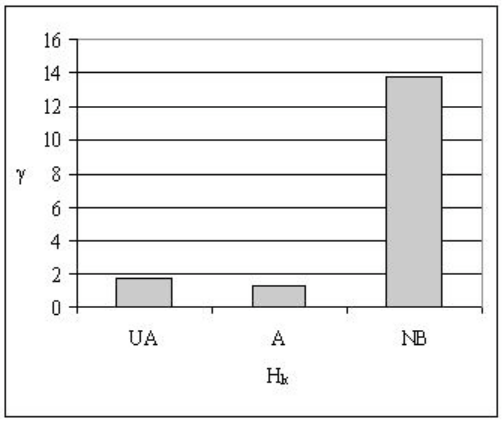

Figure 18: Medium field Q-slope values for varying thermal conductance, calculated numerically.

COMPARISON WITH EXPERIMENT

The first general observation we can make when comparing the above theoretical and numerical results with experimental data is that the thermal feedback model with standard BCS resistance generally underestimates the medium field Q-slope for frequencies below 2.5 GHz. Figure 19 summarizes the results of several measurements of γ values compiled by Ciovati [15]. The cavities represented here lie well within the range of cavity parameters considered in the previous section, yet these experimental γ values are centered around 2 or 3 while those calculated from our model are mostly less than 1. A likely cause for this discrepancy is the nonlinear BCS resistance, which we discuss below.

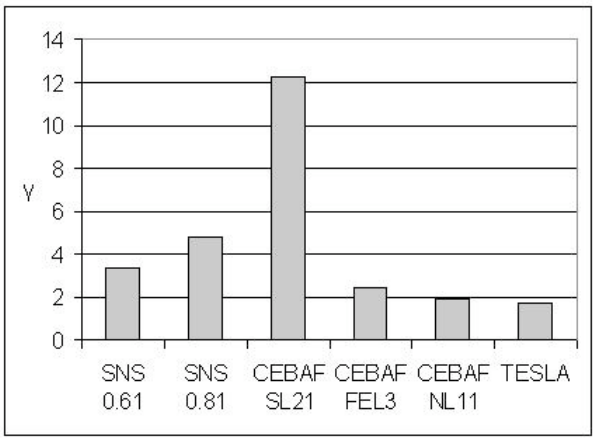

Figure 19: Values of the medium field Q-slope taken from measurements compiled by Ciovati [15]. Each value shown here is the average of a set of values obtained from measurements on a set of similar cavities. The cavities have frequencies 804 MHz (SNS), 1.5 GHz (CEBAF), and 1.3 GHz (TESLA).

In spite of this difference in scales, one can still com-

pare the general trends predicted by our model with those seen in experiment. The predicted increases in γ with increasing frequency and wall thickness and with decreasing phonon mean free path are all consistent with experimental trends [15]. However, one trend predicted by our model is strongly contradicted by experiment; while our results show γ increasing with increasing bath temperature, experimental results show the opposite. Figure 20 shows γ values obtained from measurements on a CEBAF single-cell cavity at bath temperatures 1.37 K and 2.0 K; here, the higher bath temperature leads to the lower γ value. Also shown in the figure are the results of numerical simululations we ran with parameters matching those of the CEBAF cavity; in our model, the higher bath temperature leads to the higher Q-slope. This is a significant disagreement between our thermal feedback model and experiment that needs to be addressed further. There is no indication that the inclusion of nonlinear BCS resistance in our model will resolve this discrepancy.

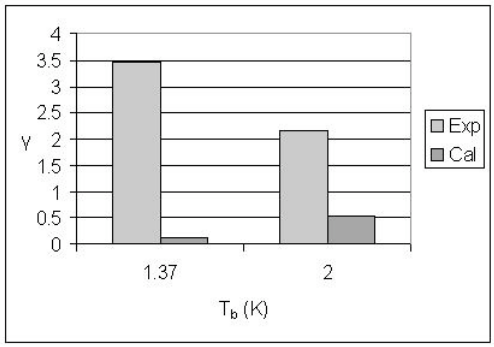

Figure 20: Comparison between data from a CEBAF cavity (light gray) and numerical simulation (dark gray).

For higher frequencies (> 2.5 GHz), the results of the standard BCS model are found to be surprisingly close to those of experimental measurements. Figure 21 shows a plot of Q vs B from measurements on a 3.9 GHz TESLA cavity [4] along with the results of a numerical simulation with matching cavity parameters. In the medium field range, the curves agree fairly well, with the simulation giving Q values only slightly higher than the data. This agreement is surprising in that, here and in other cases involving high frequency, *the nonlinear BCS theory below is not needed* to bring the simulations closer to experimental data. This agreement was also observed by Graber at 3 GHz [2].

Another interesting agreement between the numerical results and experiment can be found in the nucleate boiling regime. In Figure 17 above, we saw that numerical simulations predicted a linear ($dQ/dB \neq 0$ at $B = 0$), not quadratic, dependence of Q on B. As mentioned above, this is consistent with the fact that Halbritter's approximation and the quadratic form it implies cannot be applied to the nucleate boiling case because the thermal conductance goes to zero as the temperature difference across the Nb-

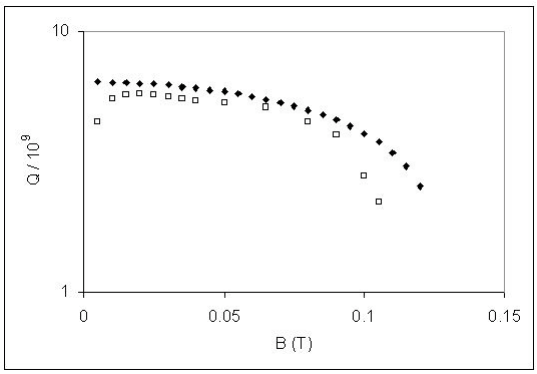

Figure 21: Measurement of Q as a function B for a 3.9 GHz TESLA cavity (□) [4] compared with the results of a numerical simulation with matching cavity parameters (⧫).

LHe interface goes to zero. The linear behavior seen in our numerical results has also been observed experimentally by Ciovati [6], as shown in Figure 22.

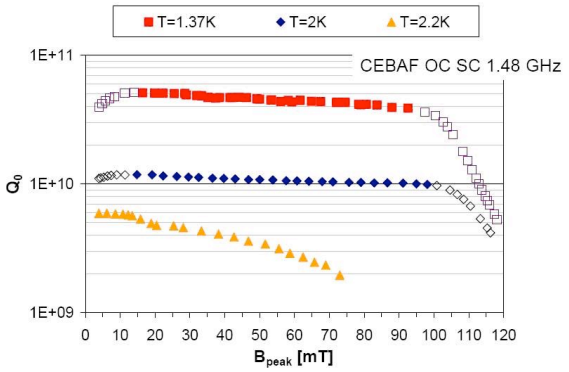

Figure 22: Measurements of Q vs B on a CEBAF cavity by Ciovati [6]. The $T = 2.2$ K curve (in yellow) is in the nucleate boiling regime and clearly shows a more linear than quadratic dependence of Q on B. (c.f. Figure 17.)

SUMMARY FOR THERMAL FEEDBACK WITH STANDARD BCS RESISTANCE

Though the standard BCS thermal feedback theory seems to underestimate the medium field Q-slope, it has demonstrated the general trends to be expected in thermal feedback effects, except possibly for the dependence of γ on the bath temperature, where theory and experimental data clearly disagree. This disagreement presents an interesting puzzle that warrants further investigation. Another such puzzle is presented by the unexpected agreement between our model and experiment found at high frequencies. One concrete result of this analysis has been a thorough confirmation of the agreement between Halbritter's approximate formula for γ and the results of numerical cal-

culations of γ.

NONLINEAR BCS RESISTANCE

There is an intrinsic nonlinear correction to the surface resistance R_s which results from the pair-breaking effect of the supercurrent density induced by the RF field [16]. The pair breaking is manifested via a change of the electron energy spectrum in a current-carrying superconductor, $E(k) = E_0(k) + v_s p_F$, where $v_s = J/en$ is the supercurrent velocity, n is the number density of superelectrons, $E_0(k)$ is the quasi-particle spectrum at $J = 0$, and p_F is the Fermi momentum. The increased density of normal electrons corresponds to a decreased gap $\Delta(v_s) = \Delta - p_F|v_s|$. Solving the kinetic equation for the distribution function of quasi-particles in a superconductor in a strong rf field allows a calculation of the current-induced RF pair breaking in the clean limit for Type II superconductors. The nonlinear surface resistance is found to increase quadratically with RF field as follows [17]:

$$R_s = \left[1 + C\left(\frac{\Delta}{k_B T}\right)^2 \left(\frac{H}{H_c}\right)^2\right] R_{s0} \qquad (54)$$

$$C = \frac{\pi^2}{384}\left[1 + \frac{\ln 9}{3\ln(4.1 k_B T \Delta \xi^2/\hbar^2\omega^2\lambda^2)}\right] \qquad (55)$$

Here H is the RF field, H_c the thermodynamic critical field, ξ the coherence length, λ the penetration depth, $\omega = 2\pi f$, and R_{s0} the standard BCS resistance. The contribution of the logarithmic term in the brackets for Nb at 2K and 2GHz is less than 8%, which allows a simpler approximate expression:

$$R_s \cong \left[1 + \frac{\pi^2}{384}\left(\frac{\Delta}{k_B T}\right)^2 \left(\frac{H}{H_c}\right)^2\right] R_s \qquad (56)$$

For Nb at 2.0 K, the factor $C(\Delta/k_B T)^2 \approx 2$.

The simple quadratic dependence is only valid for small H, typically below 40 mT at 2 K. The pair-breaking nonlinearity becomes more pronounced when $H > (T/T_c)H_c$ [18]. The full dependence is given by

$$R_s = \frac{4R_{BCS}e^{\beta_0}}{\beta_0^3(2\pi\beta_0)^{1/2}} \qquad (57)$$

$$\beta_0 = \frac{v_s p_F}{k_B T} = \frac{\pi}{2^{3/2}}\frac{H}{H_c}\frac{\Delta}{k_B T} \qquad (58)$$

and is shown in Figure 23 for H from 0 to $\approx$ 160 mT for Nb at 2 K. In this case the BCS nonlinearity can double R_s at $H_0 \approx 100$ mT as compared to R_{BCS}.

The nonlinear BCS surface resistance discussed so far is for the clean limit ($l_e \gg \xi$) only (here, l_e is the electron mean free path). Taking into account impurity scattering is a much more complicated problem but the nonlinearity in surface resistance is generally expected to decrease in the dirty limit [16].

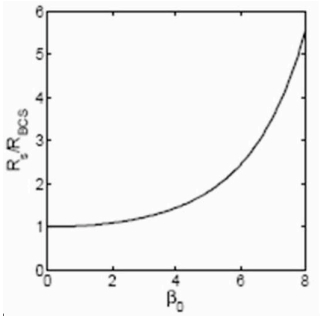

Figure 23: Increase of BCS resistance due to pair-breaking at high supercurrent density β_0 [18].

Once again we show the trends for the medium field Q-slope for changes in RF frequency, bath temperature, RRR, phonon mean free path (phonon peak), residual resistance, and wall thickness. For more accurate values of the standard BCS resistance we use the results from Halbritter's program (the SRIMP version at Cornell) instead of the Pippard approximation in Eq. (48). Figures 24-29 compare the Q vs H curves for BCS and nonlinear BCS due to variations in one of the following cavity properties while the others are held fixed at the baseline values given here:

- RF frequency f (1.3 GHz)
- Cavity wall thickness d (3.0 mm)
- Residual resistance R_0 (5 nΩ)
- Kapitza conductance H_k (annealed Nb)
- Residual resistivity ratio RRR (300)
- Helium bath temperature T_b (1.8 K)
- Phonon mean free path l (1.3 mm)
- Geometry facor G (280 Ω)

Note that this baseline set of parameters is somewhat different from the first set of baseline parameters used for the standard BCS case above in order to provide some new information. For example, the baseline phonon mean free path chosen here is 1.3 mm which will correspond to a small phonon peak in the thermal conductivity, as opposed to the previous baseline case of 0.1 mm phonon mean free path with no phonon peak. As a result, the medium field Q-slopes for the standard BCS case here are much smaller. As for the standard BCS cases, the medium field Q-slope changes more weakly with changes in wall thickness, RRR, and residual resistance.

As expected, the nonlinear BCS resistance greatly increases the medium field Q-slope over the BCS case. The strongest Q-slopes are expected for high frequencies and small phonon mean free paths. Figures 30 and 31 show the strong increase in the gamma values between the standard BCS and nonlinear BCS cases, and also the trends in gamma values for changes in phonon mean free path and rf frequency, the two strongest dependencies.

To compare these results with experimental data, we

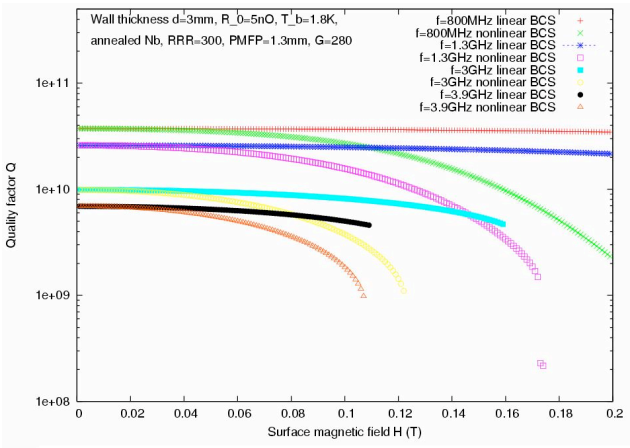

Figure 24: Variation of the cavity Q with RF surface magnetic field for RF frequencies between 800 MHz and 3900 MHz. In each case Q vs H curves are given for BCS and nonlinear BCS cases (in color).

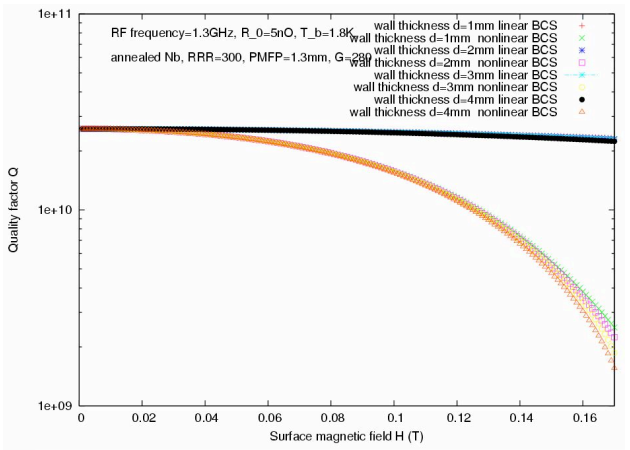

Figure 25: Variation of the cavity Q with RF surface magnetic field for cavity wall thickness between 1 mm and 4 mm. In each case Q vs H curves are given for BCS and nonlinear BCS cases (in color).

have run simulations using the nonlinear BCS resistance and matching the cavity parameters for measurements on two Cornell cavities [19], [4]; the results are shown in Figures 32 and 33. In Figure 32 we see that the numerical results and experimental data argee quite well in the medium field range; for higher fields, however, the nonlinear BCS results show a stronger Q-slope than the data. In Figure 33, the agreement is even better in the medium field range; for higher fields here, the data shows a strong high field Q-slope that cannot be reproduced by the nonlinear BCS effects.

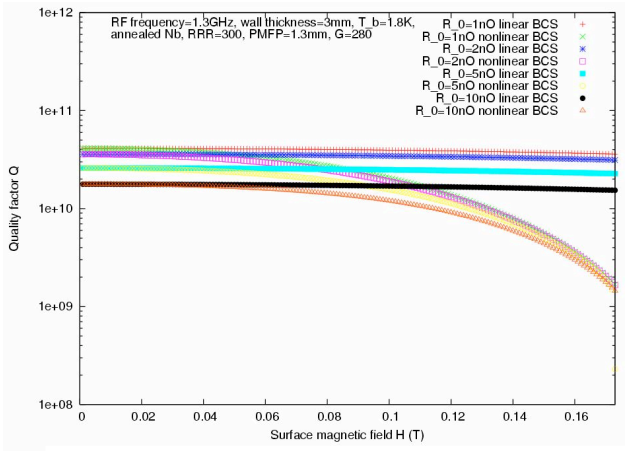

Figure 26: Variation of the cavity Q with RF surface magnetic field for residual resistance between 1 nΩ and 10 nΩ. In each case Q vs H curves are given for BCS and nonlinear BCS cases (in color).

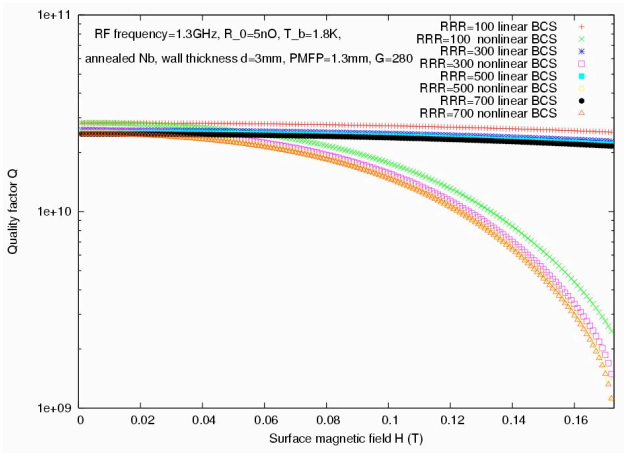

Figure 27: Variation of the cavity Q with RF surface magnetic field for RRR between 100 and 700. In each case Q vs H curves are given for BCS and nonlinear BCS cases (in color).

CONCLUSIONS

The medium field Q-slope depends on a large number of physical parameters: RF frequency, bath temperature, thermal conductivity (especially the magnitude of the phonon peak), Kaptiza conductance, wall thickness, electron mean free path (which changes due to mild baking) and residual resistance. Some of these parameters are not very well known for each cavity or even for each test, in particular the Kaptiza conductance due to baking conditions or the phonon mean free path (due to residual strains). Accurate modeling of the data requires a good knowledge of the physical parameters of the cavity, some of which are often not known to the level of detail necessary. Therefore it is useful to study the trends.

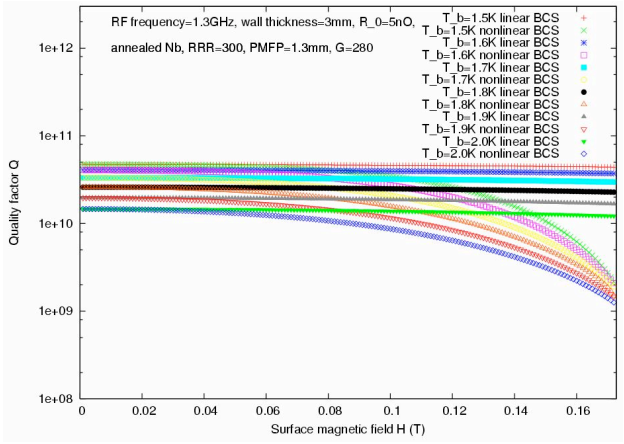

Figure 28: Variation of the cavity Q with RF surface magnetic field for bath temperatures between 1.5 and 2 K. In each case, Q vs H curves are given for BCS and nonlinear BCS cases (in color).

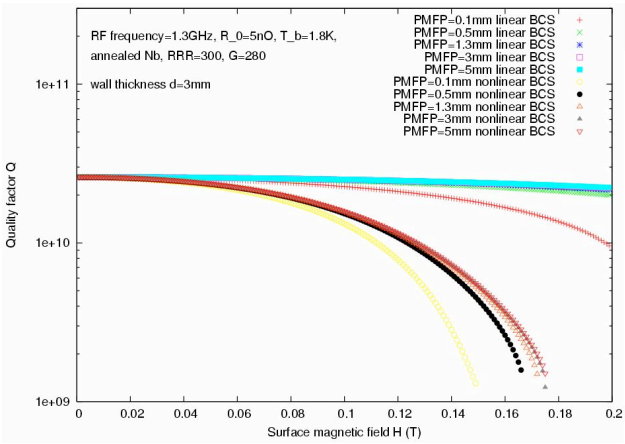

Figure 29: Variation of the cavity Q with RF surface magnetic field for phonon mean free paths between 0.1 and 5 mm. In each case Q vs H curves are given for BCS and nonlinear BCS cases (in color).

	800MHz	1.3GHz	3GHz	3.9GHz
Linear BCS	0.071	0.170	0.691	1.082
Halbritter's formula	0.077	0.178	0.716	1.089
Nonlinear BCS	0.985	1.642	3.085	3.730

Figure 30: Gamma values for BCS and nonlinear BCS for various phonon mean free paths.

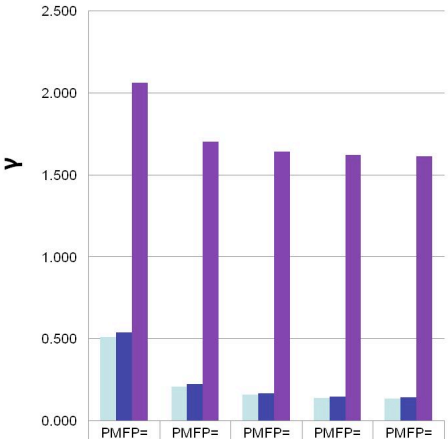

	PMFP=0.1mm	PMFP=0.5mm	PMFP=1.3mm	PMFP=3mm	PMFP=5mm
Linear BCS	0.514	0.210	0.162	0.143	0.137
Halbritter's formula	0.543	0.226	0.170	0.150	0.144
Nonlinear BCS	2.066	1.706	1.645	1.623	1.616

Figure 31: Gamma values for BCS and nonlinear BCS for various RF frequencies.

There are two striking trends in thermal feedback: one for frequency dependence and the other for phonon mean free path dependence. Post purified cavities and large grain cavities with higher thermal conductivity generally show reduced slopes primarily due to the appearance of stronger phonon peak in the thermal conductivity. For high frequency cavities the quadratic frequency dependence of the BCS surface resistance eventually results in a thermal instability well below the rf critical field (Figure 24). This has been predicted and observed as GTI in 3 GHz cavities. GTI has also been observed in 3.9 GHz [4] and for a 2.8 GHz cavity operating in the TE mode [6]. At low frequencies, however, the thermal feedback effect with standard BCS alone is much smaller and does not generally lead to a global instability. The absence of a global thermal instability for low frequency was one of the original important reasons for selecting a frequency near 1 GHz for the linear collider [20].

Inclusion of the nonlinear BCS contribution improves the fit to the medium field Q-slope for the 1.5 GHz cavity; however inclusion of the stronger high field behavior as shown in Figures 30 and 31 overestimates the medium field Q-slope as compared to the data. Similarly, for the 2.8 GHz case the nonlinear BCS quadratic term alone yields too strong a Q-slope as compared to the data. In general inclusion of the nonlinear BCS resistance often makes the medium field Q-slope stronger than the observed Q-slope [4].

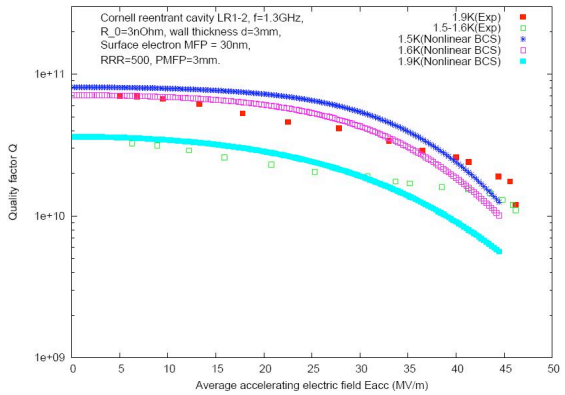

Figure 32: Q vs E_{acc} from measurements on a 1.3 GHz Cornell cavity [19], compared with the results of numerical calculations using the nonlinear BCS resistance.

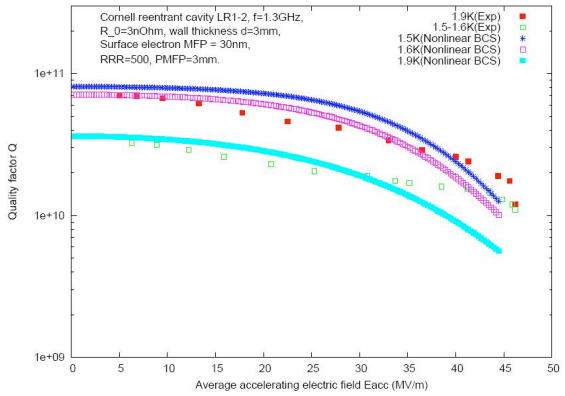

Figure 33: Q vs E_{pk} from measurements on a 1.5 GHz Cornell cavity [4], compared with the results of numerical calculations using the nonlinear BCS resistance.

REFERENCES

[1] J. Halbritter. Rf residual losses, high electric and magnetic rf fields in superconducting cavities. Superconduting materials for high energy colliders, p. 9, Eds. L Cifarelli and L. Maritato. World Scientific, 1999.

[2] J. H. Graber. High Power RF Processing Studies of 3 GHz Niobium Superconducting Accelerator Cavities. Ph.D. Thesis, Cornell University, 1993.

[3] K. Saito. Q-Slope Analysis of Niobium SC RF Cavities. Proceedings of the 11th Workshop on RF Superconductivity, Thp17, Travemunde, 2003.

[4] P. Bauer et al. Evidence for Non-Linear BCS Resistance in SRF Cavities. Proceedings of the 12th International Workshop on RF Superconductivity, TuP01, 2005.

[5] G. Ciovati. Proceedings of the 12th International Workshop on RF Superconductivity, p230, TuP02, 2005.

[6] G. Ciovati. Investigation of the superconducting properties of niobium radio-frequency cavities. Ph.D. Thesis, Old Dominion University, 2005.

[7] B. Visentin. Argonne Frontier Workshop Proceedings, p. 94, Editor K. Kim et al, 2005.

[8] H. Padamsee, J. Knobloch, and T. Hays. Superconductivity for Accelerators. John Wiley & Sons, Inc. New York, 1998.

[9] G. Ciovati and J. Halbritter. Analysis of the Medium Field Q-slope in Superconducting Cavities Made of Bulk Niobium. Proceedings of the 12th International Workshop on RF Superconductivity, TuP02, 2005.

[10] H. Padamsee. Calculations for breakdown induced by "large defects" in superconducting niobium cavities. CERN/EF/RF 82-5, 1982.

[11] F. Koechlin and B. Bonin. Parametrization of the niobium thermal conductivity in the superconducting state. Proc. of 7th Workshop on RF Superconductivity, Gif sur Yvette, France, Oct. 17 - 20, 1995, pp. 665 - 669.

[12] W. Singer. Fabrication of Single Crystal Niobium Cavities. Proceedings of the 13th International Workshop on RF Superconductivity, TuP53, 2007.

[13] K. Mittag. Cryogenics 73 (1973) 94.

[14] B. Visentin. First Results on Fast Baking. Proceedings of the 12th International Workshop on RF Superconductivity, TuP05, 2005.

[15] G. Ciovati. High Q at Low and Medium Field. Argonne Frontier Workshop Proceedings, p.52, Editor K. Kim et al, ANL-05/10 n(2005).

[16] A. Gurevich. Argonne Frontier Workshop Proceedings, p.17, Editor K. Kim et al, 2005.

[17] A. Gurevich. Thermal RF Breakdown of Superconducting Cavities. Multiscale SRF 2005 TuA01, p.156.

[18] A. Gurevich. Physica C, 441, p. 38, 2006.

[19] R. Geng. 47 MV/m World Record Accelerating Gradient Achieved in a Superconducting Niobium RF Cavity, pac 2005, Proceedings of 2005 Particle Accelerator Conference, Knoxville, Tennessee, p 653.

[20] H. Padamsee. Status Report on TESLA Activities. Proceedings of the 5th Workshop on RF Superconductivity, p. 963, Ed. D. Proch, 1991.